FOUNDATIONS OF A TWO-TEMPERATURE STATISTICAL MODEL*

by

J. R. Wayland

University of Maryland
Department of Physics and Astronomy
College Park, Maryland

February 1968

*This research was supported by the National Aeronautics and Space Administration under Grant NsG-695.

Abstract

The recent secondary particle spectra from proton-proton interactions at machine energies were analyzed by the two-temperature statistical model of Wayland and Bowen to test for the independence of the longitudinal and transverse momentum (P_ℓ and P_t, respectively). It was found that the assumption of independence of P_ℓ and P_t is consistent with experiments. The variation of the longitudinal temperature with incident energy is considered in detail. The energy variation of the multiplicity of particles as a function of incident energy is found to be in agreement with cosmic ray results. The parameters for fitting particle spectra are given.

I. INTRODUCTION

In the last few years, detailed information of the shape of particle spectra from proton-proton and proton-nuclei interactions at energies greater than 10 GeV has become available. Thus, it is possible to check various models for particle production more carefully. The lack of success of older models led to attempted new models that rely more on phenomenological observations.[1-5] A guiding principle that has played a dominant role is the apparent independence of the transverse momentum distribution of produced particles from the incident energy of the incoming particle.[1-4] Imeda[6] has made a careful analysis that seems to indicate only one of the proposed transverse momentum distributions gives a satisfactory fit. Independently, Wayland and Bowen[4] and Hagedorn[2] had obtained the same results. Using the independency of the transverse momentum distribution, Wayland and Bowen[4] developed a two-temperature model. A basic assumption of the model is that the distribution function of the secondary particles can be written as $f(P_t^*)$ $g(P_\ell^*)$; i.e. that P_t^* (the transverse momentum) and P_ℓ^* (the longitudinal momentum) are independent variables. The recent BNL[7] results indicate that there are strong experimental grounds for this assumption. With this in mind, we re-examined the experimental data. Generally we find that the two-temperature model gives good fits to experimental data. The analytic form of the two-temperature model allows easy extension of the predictions to cosmic ray energies.

In Section II we will give the main features of the two-temperature model.[4] Using the results of Section II we examine, in Section III, proton spectra from N-N interactions. We then indicate how to extend the calculations to other incident energies. In Sections IV and V we consider pion, kaon and antiproton spectra. Finally the energy variation of particle multiplicites as predicted by the model agrees with cosmic ray results.

II. THE TWO TEMPERATURE MODEL

The main assumption of the two-temperature model is that there are two characteristic temperatures: one is associated with the transverse momentum distribution (T_o), the other with the longitudinal momentum distribution (T). The temperature, T, can be considered as the quasi-equilibrium condition at which the various particles "boil off" as the interaction volume cools. We start with quantum-statistical mechanical average occupation number density.

$$\bar{v} = \frac{1}{\exp[\sqrt{P^2 + m^2}/T] \pm 1} , \tag{1}$$

where P and m are the momentum and mass of the particles. We use the convention of the negative sign for bosons and the positive sign for fermions. The normalized momentum distributions are:

$$W_\ell^{(N)}(P_\ell^*)dP_\ell^* = \frac{T}{m^2c^3} \frac{\sum_{k=1}^{\infty} (\pm)^{k+1}[\exp(-\frac{k\mu_1}{T})/k^{3/2}][1 + \frac{k\mu_1}{T}]}{\sum_{k=1}^{\infty} (\pm)^{k+1}K_2(kmc^2/T)/k} dp_\ell^* \tag{2}$$

$$W_t^{(N)}(P_t^*)dP_t^* = \frac{P_t^*\mu_2}{T_o m^2c^2} \frac{\sum_{k=1}^{\infty} (\pm)^{k+1}K_1(k\mu_2/T_o)}{\sum_{k=1}^{\infty} (\pm)^{k+1}K_2(kmc^2/T_o)/k} dp_t^* \tag{3}$$

where

$$\mu_1^2 = P_\ell^{*2} + m^2,$$

$$\mu_2^2 = P_t^{*2} + m^2,$$

and the K's are modified Bessel functions of the second type. With the assumption that the longitudinal temperature determines the number of particles, n, we have

$$n = \frac{V_o m^2 cT}{h^3} \sum_{k=1}^{\infty} (\pm)^{k+1} \frac{K_2(\frac{kmc^2}{T})}{k}, \tag{4}$$

where

$$V_o \equiv \frac{4}{3}\pi(\frac{\alpha hc}{T_o})^2(\frac{\alpha hc}{T}).$$

Thus the flux of particles is given by

$$\frac{d^2N}{dP_t^* dP_\ell^*} = \frac{V_o}{T_o m^2 c^4 h^3} P_t^* T^2 \mu_2 \frac{\sum_{k=1}^{\infty} (\pm)^{k+1} K_1(\frac{k\mu_2}{T_o}) \sum_{k=1}^{\infty} (\pm)^{k+1} \exp(\frac{-k\mu_1}{T})(1 + \frac{k\mu_1}{T})/k^{3/2}}{\sum_{k=1}^{\infty} (\pm)^{k+1} K_2(kmc^2/T_o)/k} \tag{5}$$

or

$$\frac{d^2N}{dP^* d\Omega^*} = \frac{2V_o T^4}{T_o m^2 c^4 h^3} (\frac{P^*}{T})^2 \mu_2 \frac{\sum_{k=1}^{\infty} (\pm)^{k+1} K_1(\frac{k\mu_2}{T_o}) \sum_{k=1}^{\infty} (\pm)^{k+1} \exp(\frac{-k\mu_1}{T})(1 + \frac{k\mu_1}{T})/k^{3/2}}{\sum_{k=1}^{\infty} (\pm)^{k+1} \frac{K_2(kmc^2/T_o)}{k}} \tag{6}$$

We also find for the average values of the transverse and longitudinal momentum

$$\langle P_t^* \rangle = \left(\frac{\pi m T_o}{2}\right)^{1/2} \frac{K_{5/2}(m/T_o)}{K_2(m/T_o)} , \tag{7}$$

and

$$\langle P_\ell^* \rangle = \left(\frac{2mT}{\pi}\right)^{1/2} \frac{K_{5/2}(m/T)}{K_2(m/T)} . \tag{8}$$

We know experimentally the value for $\langle P_t \rangle$ for various particles. This allows us to determine the value of T_o for each particle. Then by varying V_o and T, we can fit experimental results at a given incident energy and secondary particle angle. (We note that we require three parameters.) Then using Eqn. (5) or (6), we can predict the results at different angles. In Section III we show how to extend the results to different incident energies. We make the usual assumption that to find $d^2\sigma/dP^*d\Omega^*$ we multiply $d^2N/dP^*d\Omega^*$ by the inelastic cross section, σ_{in}.

III. PROTON SPECTRA

Let us now consider the proton spectra from proton-proton interactions at 30 GeV/c. With $T_o = 0.12 \pm 0.002$ GeV, $T = 5.0 \pm 0.3$ GeV and $\alpha = 0.43 \pm 0.01$, we find a fit to the proton spectra shown in Fig. I. The fit is not particularly sensitive to the value of T. There is good agreement for all angles and secondary momentum. (One does not expect to fit the diffraction peaks.)

If we can separate the expression for the cross section for the variables P_t^* and P_ℓ^*, we would expect that $d^2\sigma/dP^* dP_\ell^*$ as a function of P_ℓ^* at a fixed P_t^* to follow the expression for $W_\ell(P_\ell^*)$. Using the same parameters as above, we obtain Fig. II. We notice that the curves are relatively flat from .2 GeV/c to 3.0 GeV/c. Thus if we plot $d^2\sigma/dP_t^* dP_\ell^*$ as a function of P_t^* for 0.2 GeV/c $\leq P_\ell^* \leq$ 3.0 GeV/c, we would expect it to follow the expression for $W_t(P_t^*)$. The results using the above values for T_o and T are shown in Fig. III. The curves are for $P_\ell^* = 0.2$ and 3.0 GeV/c. Thus there is a strong confirmation of the assumption that we can treat P_t^* and P_ℓ^* as independent variables.

To extend our results to other values of the incident momentum, we must find how T varies. Keeping T_o fixed, consider

$$n_s \langle E_s^* \rangle = K_s^* E_o^* , \tag{9}$$

where n_s is the average number of secondaries, s, produced, $\langle E_s^* \rangle$ is the average energy per particle of the secondaries, K_s^* is the fraction of the total energy content of system associated with the secondary, s, and E_o^* is the total energy content. We can obtain an expression for $\langle E_s^* \rangle$ directly from Eqns. (1) and (4):

$$n_s\langle E_s\rangle = \frac{\left[\sum_{k=1}^{\infty} (\pm)^{k+1} \phi_s\left(\frac{km_sc^2}{T_s}\right)/k^3\right] 2\pi V_o t T_s^3}{h^3 c} \tag{10}$$

where

$$\phi_s\left(\frac{km_s}{T_s}\right) \equiv \Gamma(3) \int_o^{\infty} \exp\left(-\frac{k\mu_1}{T_s}\right)\left(1 + \frac{k\mu_1}{T_s} + \frac{k^2\mu_1^2}{2T_s^2}\right)dp_\ell$$

When we insert Eqn. (10) into Eqn. (9), we find that

$$\frac{2\pi V_o t}{h^3 c} T_s^3 \sum_{k=1}^{\infty} \frac{(\pm)^{k+1}}{k^3} \phi_s\left(\frac{km_sc^2}{T_s}\right) = K_s^* E_o^* . \tag{11}$$

By numerical integration, we can find how E_s^* is related to m and T. If we let

$$\Phi_s\left(\frac{m_sc^2}{T_s}\right) \equiv \sum_{k=1}^{\infty} \frac{(\pm)^{k+1}}{k^3} \phi_s\left(\frac{km_sc^2}{T_s}\right) \tag{12}$$

we can plot $\Phi_s\left(\frac{mc^2}{T}\right)$ as a function of T and m. The results are shown in Fig. IV (We have kept the first eight terms.). Thus in the case of protons, $\Phi \sim T$, and we can write $T = \text{const}\ (E_o^*)^{1/4}$.

Using this variation for T, we compare our prediction with the experimental results at incident momenta of 10 and 20 GeV/c in Fig. V. The results are good at 20 GeV/c. However, we notice that the model does not fit at 10 GeV/c. We should expect this; however, because at energies less than 15 GeV/c the transverse and longitudinal momentum distributions are very similar.

Then there would not be a decoupling and the two-temperature concept is invalid. The results at zero degrees at 18.8 and 23.1 GeV/c are shown in Fig. VI.

IV. PION SPECTRA

When we fit the $\pi^{\pm}$ production spectra in pp collisions at 30 GeV/c,[7,8] we find that $T_o = 0.14 \pm 0.005$ GeV and $T_{\pi+} = .48 \pm 0.01$ GeV, $T_{\pi-} = .40 \pm 0.01$ GeV and $\alpha_{\pi+} = 1.31 \pm 0.01$, $\alpha_{\pi-} = 1.42 \pm 0.01$ give the results shown in Figs. VII and VIII. We have taken into account the 50% target efficiency for the earlier data and assume $\sigma_{in} \simeq 30$ mb at 30 GeV. The fit is good over a wide range of angles and secondary momenta.

In obtaining the above fit to the data, we have introduced a variation in the interaction volume, V_o (i.e. normalization constant), that is dependent upon the C. M. Angle. To show how this might arise, let us extend the usual concept involved in the overlap function. Consider two nucleons that just overlap. When the overlap volume reaches some minimum value, we would expect the mesonic clouds surrounding the cores to produce a meson. (Fig. IXa). This then is the minimum interaction volume V_o'. As the overlap volume increases, the cores begin to interact with the mesonic clouds. This is probably a more efficient method of producing mesons than a meson cloud--meson cloud interaction (Fig. IXb). When there is a complete overlap (Fig. IXc), the cores are interacting and the mesonic clouds are interacting. Under this condition, the production of mesons will decrease and the production of protons will increase. Thus, we would expect the interaction volumn for mesons to go through a maximum. We can estimate this maximum by noting that for N stochastic momentum vectors the probability distribution for their sum becomes gaussian for large N. It is found that a best fit is obtained for a gaussian volume distribution superimposed upon the minimum volume V_o';

$$V_o = V_o' \left[1 + \frac{k'}{\sigma\sqrt{2\pi}} \exp\left\{ \frac{-\langle p^* \rangle^2}{2\sigma^2} \left[1 - \cos(2\langle \theta^* \rangle - \theta) \right]^2 \right\} \right] , \qquad (13)$$

where

$$\tan \langle \Theta^* \rangle = \frac{\langle P_t^* \rangle}{\langle P_\ell^* \rangle} = \frac{\pi}{2} \sqrt{\frac{T_o}{T} \frac{K_2(m/T)\ K_{5/2}(m/T_o)}{K_2(m/T_o)\ K_{5/2}(m/T)}} \quad , \tag{14a}$$

and

$$\langle P^* \rangle^2 = \langle P_t^* \rangle^2 + \langle P_\ell^* \rangle^2 \ ,$$

$$\sigma = 0.05 \pm 0.002 \text{ GeV/c},$$

$$k' = 0.17 \pm 0.01 \text{ GeV/c } (\pi^+). \tag{14b}$$

The fit is not radically altered if we assume V_o is constant.

Using the same parameters, we can fit the data for pions in the $d^2\sigma/dP_t^*\, dP_\ell^*$ *vs.* P_ℓ^* as shown in Fig. II.

When we examine Fig. IV, we see that again we can assumt $T = \text{const } (E_o^*)^{1/4}$. In fact if we set $\bar{n}_{\pi^-} \simeq 1.7$ at 30 GeV, we can find $K^*_{\pi^\pm}$ (the "inelasticity") from the knowledge of $\langle P_t^* \rangle$, $\langle P_\ell^* \rangle$ and E_o^*. This gives $K^*_{\pi^+} = 0.16$ and $K^*_{\pi^-} = 0.14$. Using this information we extend our results to 23.1, 20, 18.8 and 10 GeV/c incident momenta. (Fig. 10 thru 13) We notice that the 10 GeV/c and 0° at 18.8 and 23.1 GeV/c do not agree. The lack of a fit at 10 GeV/c is expected. The disagreement at 0° probably results from a process that does not establish a thermodynamical quasiequilibrium.

V. KAON AND ANTIPROTON SPECTRA

When the above approach is applied to K^+, K^- and $\bar{p}$ spectra from BNL at 30 GeV, the best results are obtained for the choice of the parameters given in Table I. To obtain the inelasticities we have assumed that $n_{K^-}/n_{\pi^-} \simeq 0.04$, $n_{K^+}/n_{\pi^-} \simeq 0.12$ and $n_{\bar{p}}/n_{\pi^-} \simeq 10^{-2}$. Using the same analysis as above, we extend the calculations to 18.8 and 23.1 GeV/c. The results are shown in Figs. 14 through 17.

VI. MULTIPLICITY

One way of checking the validity of this model at higher energies is to calculate the expected multiplicity of particles produced at very high energies. Using Eqn. (4) we find that the multiplicity is given by

$$N = \sum_s N_s = \sum_s \frac{(V_o)_s m_s^2 c T_s}{h^3} \sum_{k=1}^{\infty} (\pm)^{k+1} \frac{K_2(\frac{km_s c^2}{T_s})}{k} \qquad (15)$$

If we use the values for T, V_o determined for the above particles, we obtain the results shown in Fig. XVIII.* We have included $N \sim E_o^{1/4}$ for comparison (the dotted line). Thus, Eqn. (4) will tend to give an upper limit. Because of the way we have defined our cross section, this indicates that the results at higher energies will be maximal.

---

* For pions we have used an average V_o.

VII. PARTICLE SPECTRA AT 70 GeV/c

The pion and proton spectra at 10 mr and 100 mr and an incident energy of 70 GeV/c are shown in Fig. XIX.

VIII. DISCUSSION

Using the two-temperature model we have examined particle spectra from proton-proton and proton-nuclei interactions at machine energies. We find that:

(a) the assumption of independence of the transverse and longitudinal momenta at high energies is experimentally justified;

(b) the extension of calculations to higher energies by $T \sim$ (total C.M. energy)$^{1/4}$ is consistent with measured multiplicities;

(c) by keeping the first few terms in the summations, the low momenta, low angle data is more closely fitted;

(d) the pion data at 0° cannot be explained by a set of parameters that is consistent with the nonzero degree data.

The validity of the assumption of independence of P_t^* and P_ℓ^*, (a), allows one to estimate quickly the average transverse and longitudinal momenta. By fitting $d^2\sigma/dP_t^* \, dP_\ell^*$ as a function of P_ℓ^* and P_t^*, the values of T_o and T can be obtained. Then $\langle P_t^* \rangle$ and $\langle P_\ell^* \rangle$ are found with the aid of Eqn. (7) and (8). The agreement with the observed multiplicities does not establish the two-temperature model (b). Only with more accurate measurements in the very high energy range will this question be answered. In the first paper on the two-temperature model[4], the problem of low momentum, small production angle secondary particles was discussed. It was pointed out that the discrepancy probably results from the large number of particles produced in the backward direction from nucleon-complex nuclei interactions. The marked change in the shape of the pion spectra in the direction of the forward axis probably results from a process that does not fit into the quasi--equilibrium of the two-temperature model. Thus for (d) we cannot expect agreement.

IX. CONCLUSION

The analysis of recent experimental particle spectra from nucleon--nucleon interactions indicates the basic assumption of the independence of the transverse and longitudinal momenta in the two-temperature model is valid. The predictions indicate that one can extend calculations of particle production to higher energies by simple considerations that are based upon physically understandable conditions.

ACKNOWLEDGEMENTS

I would like to thank M. La Pointe and G. Yodh for many interesting discussions. E. W. Anderson kindly sent large scale graphs of the recent BNL results.

TABLE I

Parameters of two-temperature model at incident energy of 30 GeV

Particle	T_o(GeV)	T(GeV	K	$\langle\theta^*\rangle$(radians)	k'(GeV/c)	σ(GeV/c)	α
π^+	0.14[a]	0.48	0.18	0.45	0.17	0.05	1.31
π^-	0.14[a]	0.40	0.16	0.52	0.17	0.05	1.42
K^+	0.115[a]	0.32	0.0081	0.54	0.17	0.05	0.86
K^-	0.115[a]	0.21	0.0066	0.81	0.17	0.05	1.10
P	0.12[b]	5.0	--	--	--	--	0.43
$\bar{P}$	0.14[c]	0.17	0.0022	--	--	--	0.32

(a) This was obtained from the results given by Imaeda[6] for $\langle P_t \rangle$.

(b) This was obtained from $\langle P_t \rangle$ for protons of 475 MeV/c.

(c) This was obtained from the results given by Dekkers, et. al.[9] for $\langle P_t \rangle$.

REFERENCES

[1] G. Cocconi, D. H. Perkins and L. J. Koester: Study No. 28 of Berkeley High-Energy Physics Study, UCRL - 10022 (unpublished).

[2] R. Hagedorn: Suppl. Nuovo Cimento, 3, 147 (1965).

[3] R. Hagedorn and J. Ranft: CERN - Th. 851 (to be published); R. Hagedorn: CERN - Th. 751 (to be published).

[4] J. R. Wayland and T. Bowen: Nuovo Cimento 48A, 663 (1967).

[5] G. Trilling: UCRL 16000 (unpublished).

[6] K. Imaeda: Nuovo Cimento, 48A, 482 (1967).

[7] E. W. Anderson, et. al.: Phys. Rev. Lett. 19, 198 (1967).

[8] W. T. Baker, et. al.: Phys. Rev. Lett. 7, 101 (1961).

[9] D. Dekkers, et. al.: Phys. Rev., 137, B962 (1965).

[10] D. H. Perkins, Proc. Int'l. Conf. Theor. Aspects of Very High-Energy Phenomena, CERN 61-22 (1961).

FIGURE CAPTIONS

Fig. 1 - Momentum Spectra of Protons at an Incident Momentum of 30 GeV/c.[7]

Fig. 2 - Momentum Spectra of Particles for P_{ℓ}^{*} at an Incident Momentum of 30 GeV/c. [7]

Fig. 3 - Momentum Spectra of Protons for P_{t}^{*} at an Incident Momentum of 30 GeV/c. [7]

Fig. 4 - The Function Φ_s (mc^2/T) vs. T for Various Values of m.

Fig. 5 - Momentum Spectra of Protons at Incident Momentum of 10 and 20 GeV/c. [7]

Fig. 6 - Momentum Spectra of Protons at Incident Momentum of 18.8 and 23.1 GeV/c.[9]

Fig. 7 - Momentum Spectra of Pions at Incident Momentum of 30 GeV/c.[7]

Fig. 8 - Momentum Spectra of Pions at Incident Momentum of 30 GeV/c (50% Target Efficiency). [7]

Fig. 9 - The Interaction Volume as a Function of the Overlap of the Interacting Nucleons.

Fig. 10 - Momentum Spectrum of π^+ at incident momentum of 18.8 and 23.1 GeV/c. [9]

Fig. 11 - Momentum Spectra of π^- at Incident Momentum of 18.8 and 23.1 GeV/c.

Fig. 12 - Momentum Spectra of π^- at Incident Momentum of 20 GeV/c (50% Target Efficiency). [8]

Fig. 13 - Momentum Spectra of Pions At Incident Momentum of 10 GeV/c (50% Target Efficienty). [8]

Fig. 14 - Momentum Spectra of K^+ at Incident Momentum of 18.8 and 23.1 GeV/c. [9]

Fig. 15 - Momentum Spectra of K^- at Incident Momentum of 18.8 and 23.1 GeV/c. [9]

Fig. 16 - Momentum Spectra of Antiprotons at Incident Momentum of 30 GeV/c (50% Target Efficiency).[8]

Fig. 17 - Momentum Spectra of Antiprotons at Incident Momentum of 23.1 GeV/c. [9]

Fig. 18 - The Average Number of Charge Particles Produced by Interaction of Protons and Pions. [10]

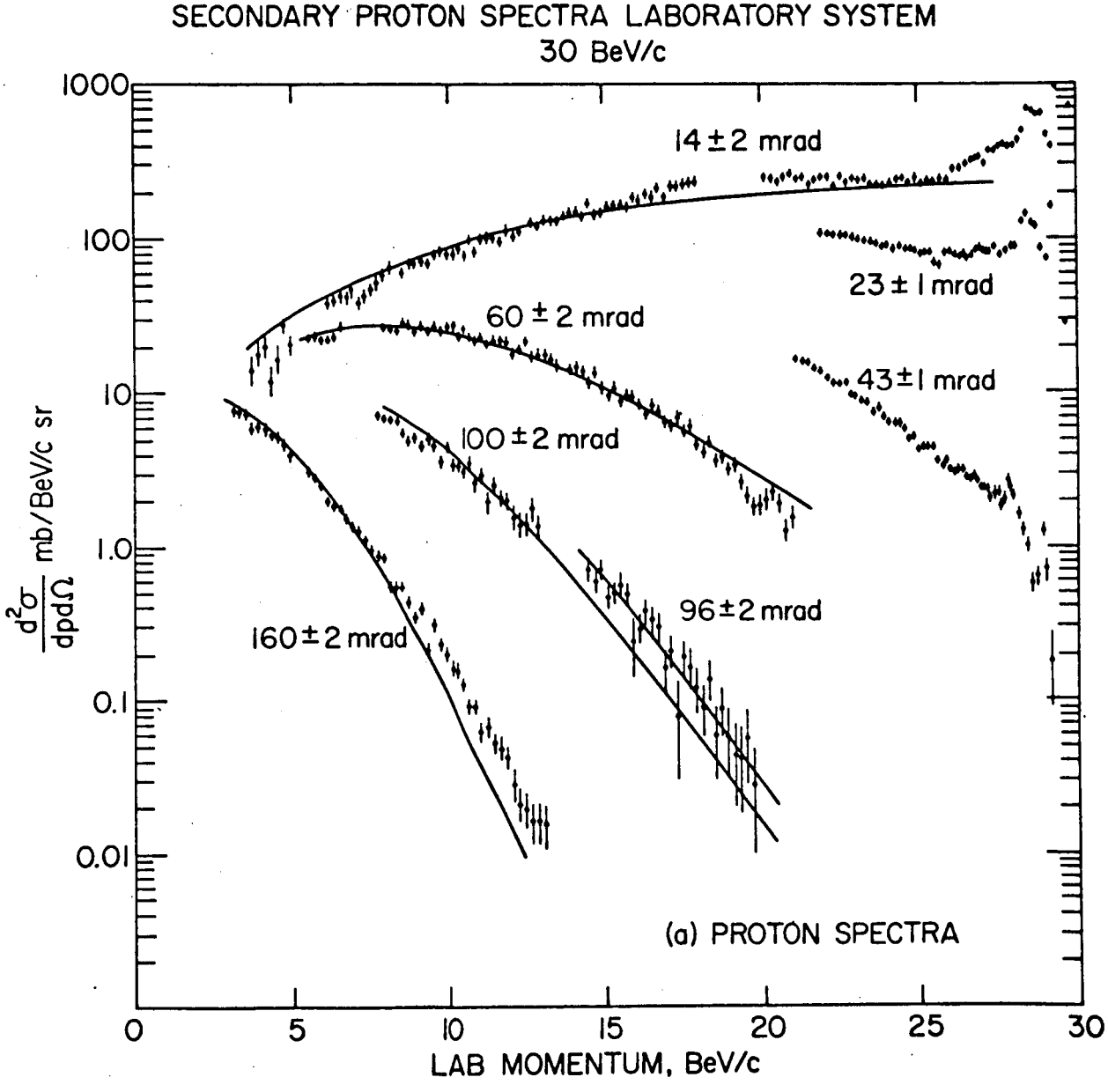
SECONDARY PROTON SPECTRA LABORATORY SYSTEM
30 BeV/c
1000
100
10
1.0
0.1
0.01
$\frac{d^2\sigma}{dpd\Omega}$ mb/BeV/c sr
14 ± 2 mrad
23 ± 1 mrad
60 ± 2 mrad
43 ± 1 mrad
100 ± 2 mrad
96 ± 2 mrad
160 ± 2 mrad
(a) PROTON SPECTRA
0
5
10
15
20
25
30
LAB MOMENTUM, BeV/c

Fig. 1

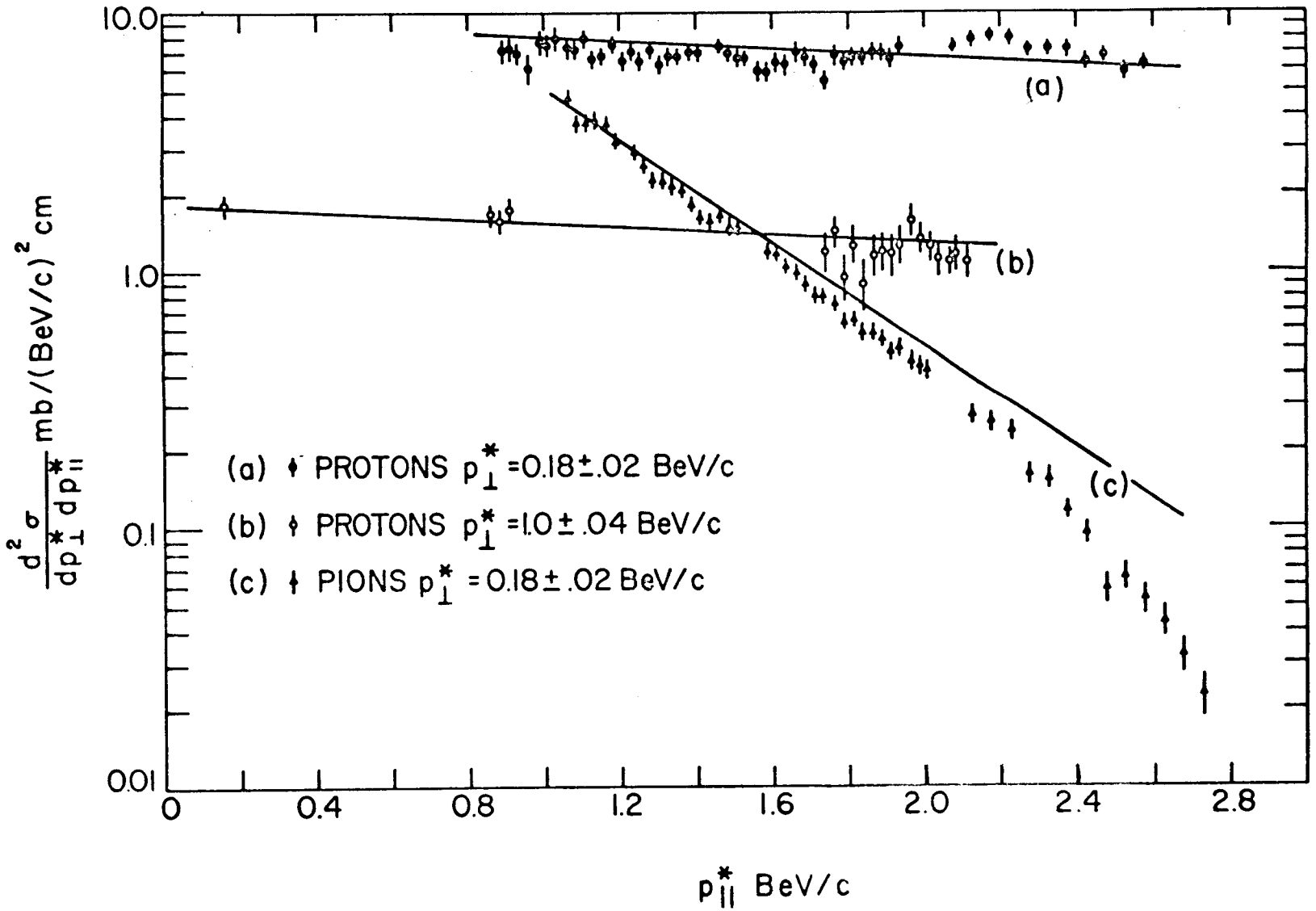
10.0
1.0
0.1
0.01
0
0.4
0.8
1.2
1.6
2.0
2.4
2.8
$\frac{d^2\sigma}{dp_\perp^* dp_{||}^*}$ mb/(BeV/c)^2 cm
$p_{||}^*$ BeV/c
(a)
(b)
(c)
(a) PROTONS $p_\perp^*$ =0.18±.02 BeV/c
(b) PROTONS $p_\perp^*$ =1.0±.04 BeV/c
(c) PIONS $p_\perp^*$ =0.18±.02 BeV/c

Fig. 2

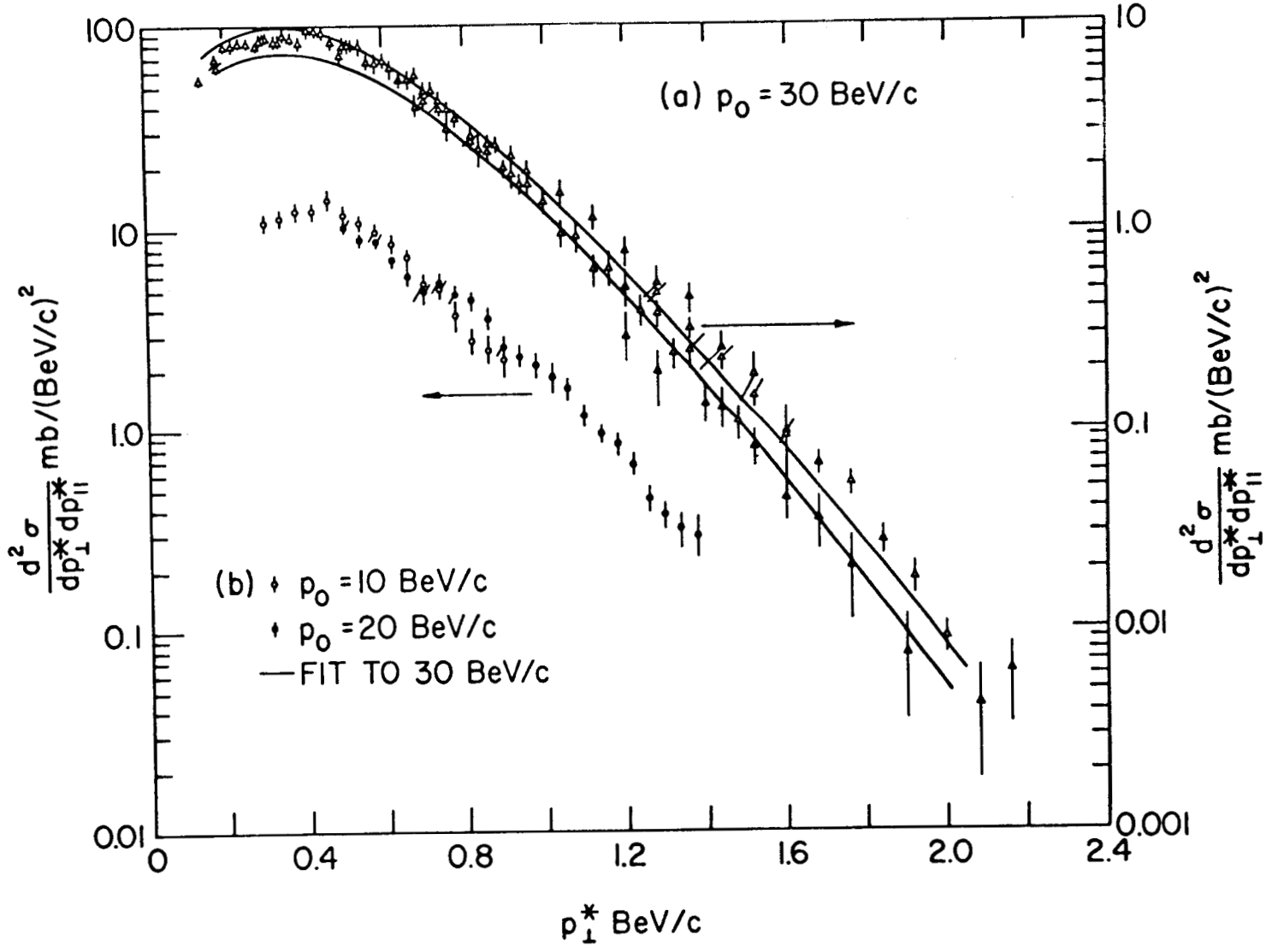
(a) p_0 = 30 BeV/c
(b) p_0 = 10 BeV/c
p_0 = 20 BeV/c
—FIT TO 30 BeV/c
$\frac{d^2\sigma}{dp_\perp^* dp_{11}^*}$ mb/(BeV/c)^2
$p_\perp^*$ BeV/c
100
10
1.0
0.1
0.01
0
0.4
0.8
1.2
1.6
2.0
2.4
10
1.0
0.1
0.01
0.001

Fig. 3

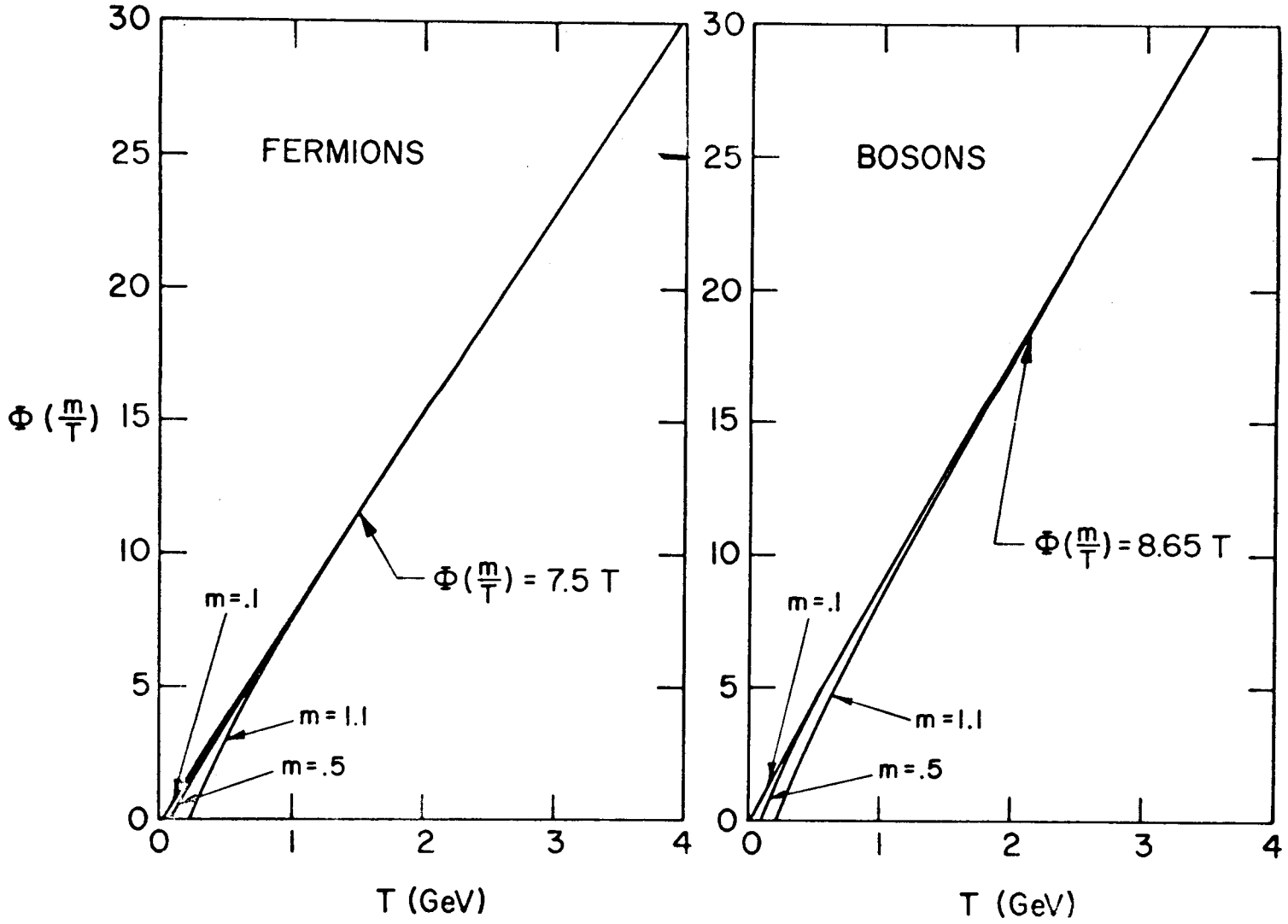
FERMIONS
BOSONS
Φ(m/T)
Φ(m/T) = 7.5 T
Φ(m/T) = 8.65 T
m=.1
m=.5
m=1.1
T (GeV)
0
5
10
15
20
25
30
1
2
3
4

Fig. 4

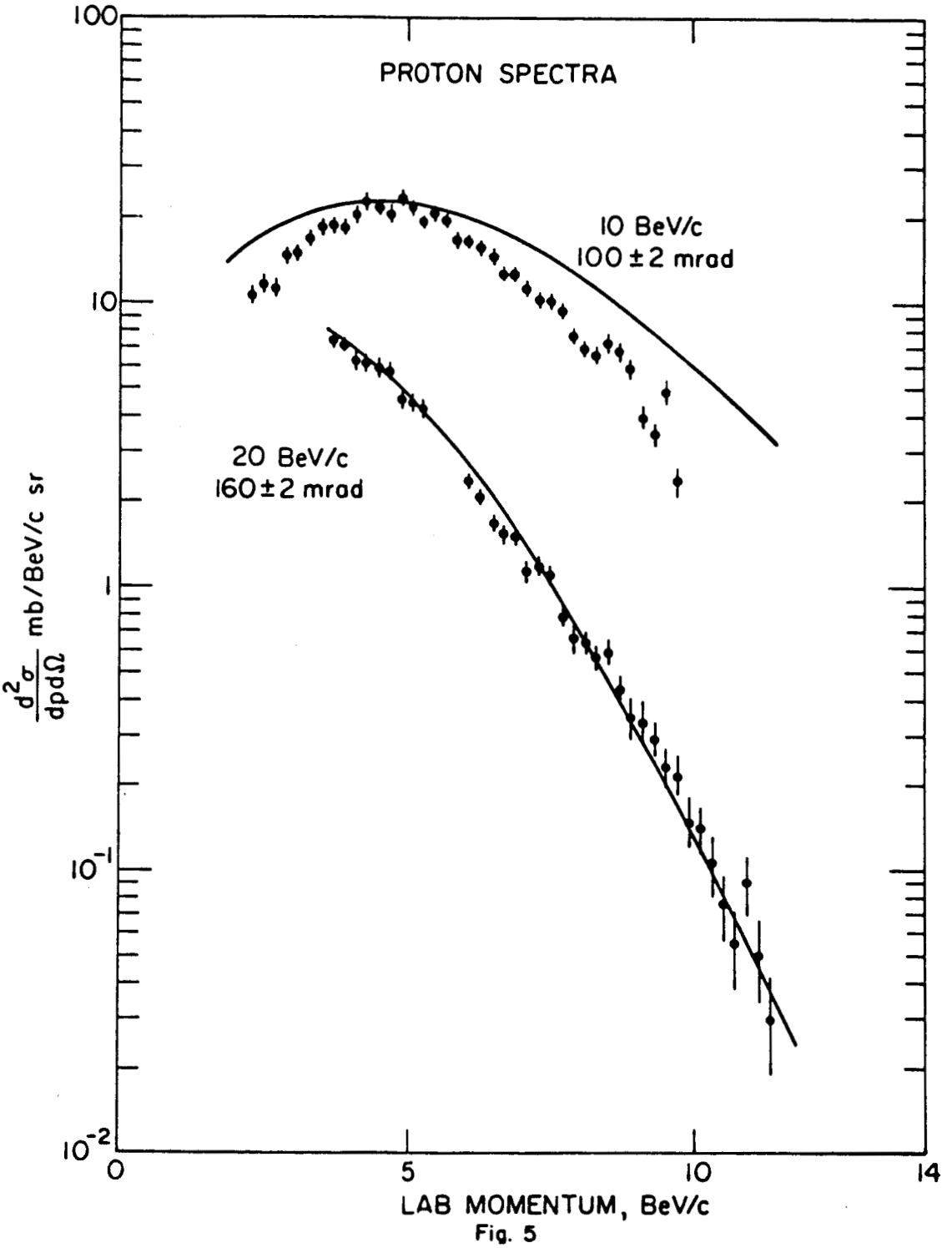
PROTON SPECTRA
10 BeV/c
100 ± 2 mrad
20 BeV/c
160 ± 2 mrad
100
10
1
10^{-1}
10^{-2}
$\frac{d^2\sigma}{dpd\Omega}$ mb/BeV/c sr
0
5
10
14
LAB MOMENTUM, BeV/c

Fig. 5

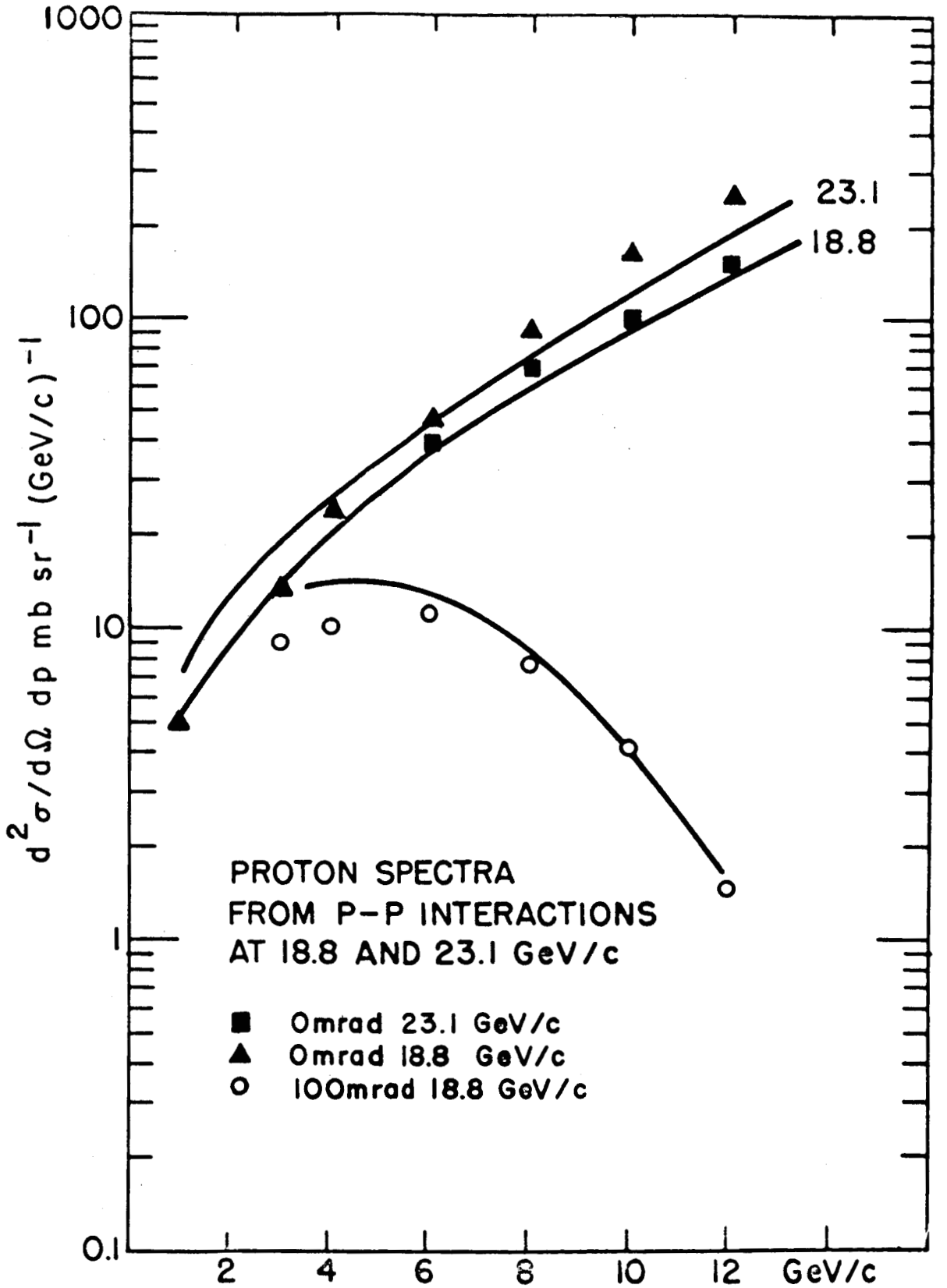
1000
100
10
1
0.1
$d^2\sigma/d\Omega\ dp$ mb sr^{-1} $(GeV/c)^{-1}$
23.1
18.8
PROTON SPECTRA
FROM P-P INTERACTIONS
AT 18.8 AND 23.1 GeV/c
Omrad 23.1 GeV/c
Omrad 18.8 GeV/c
100mrad 18.8 GeV/c
2
4
6
8
10
12
GeV/c

FIG. 6

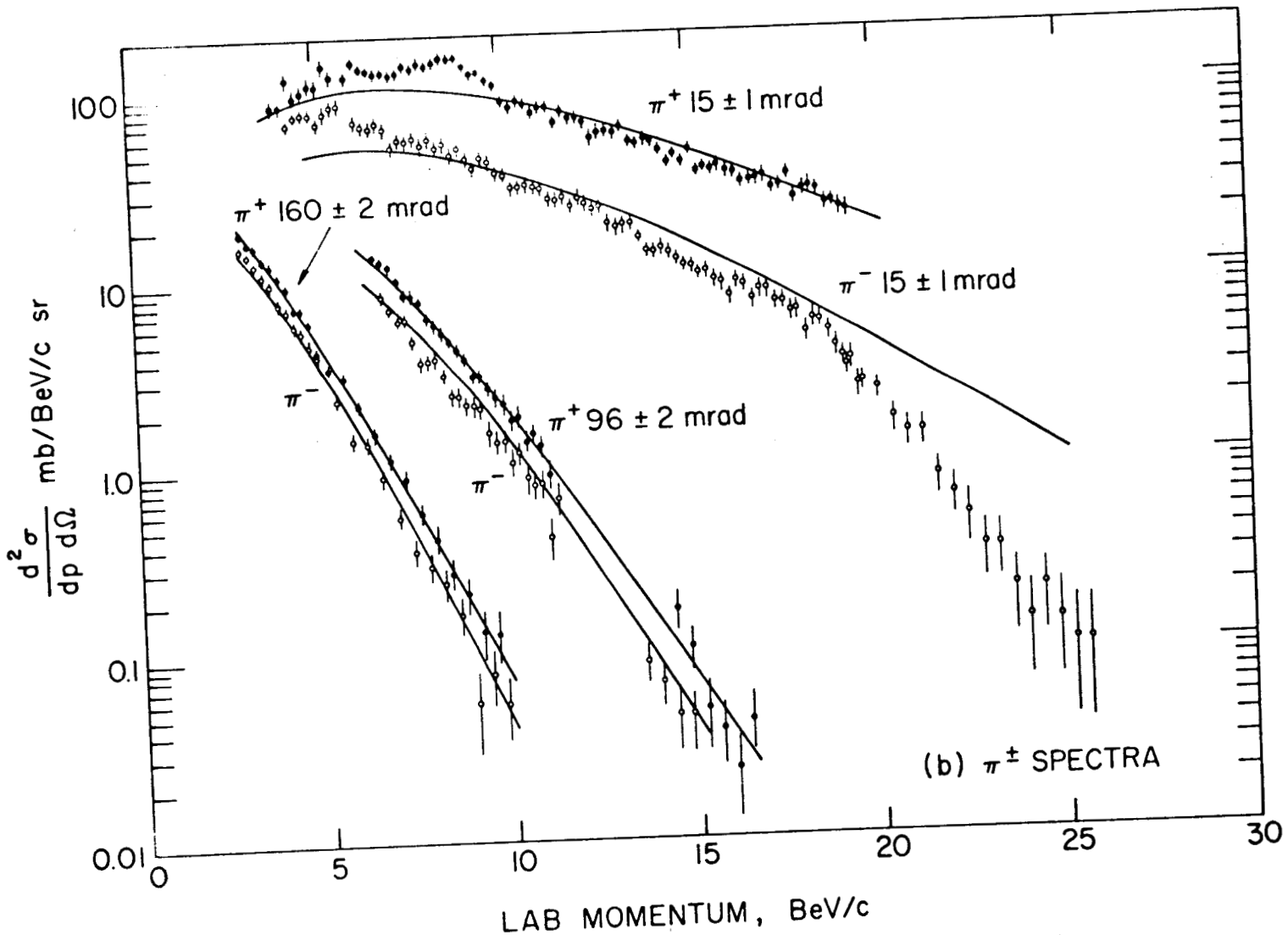
100
10
1.0
0.1
0.01
0
5
10
15
20
25
30
$\frac{d^2\sigma}{dp\,d\Omega}$ mb/BeV/c sr
LAB MOMENTUM, BeV/c
π^+ 15 ± 1 mrad
π^- 15 ± 1 mrad
π^+ 160 ± 2 mrad
π^-
π^+ 96 ± 2 mrad
π^-
(b) $\pi^\pm$ SPECTRA

Fig. 7

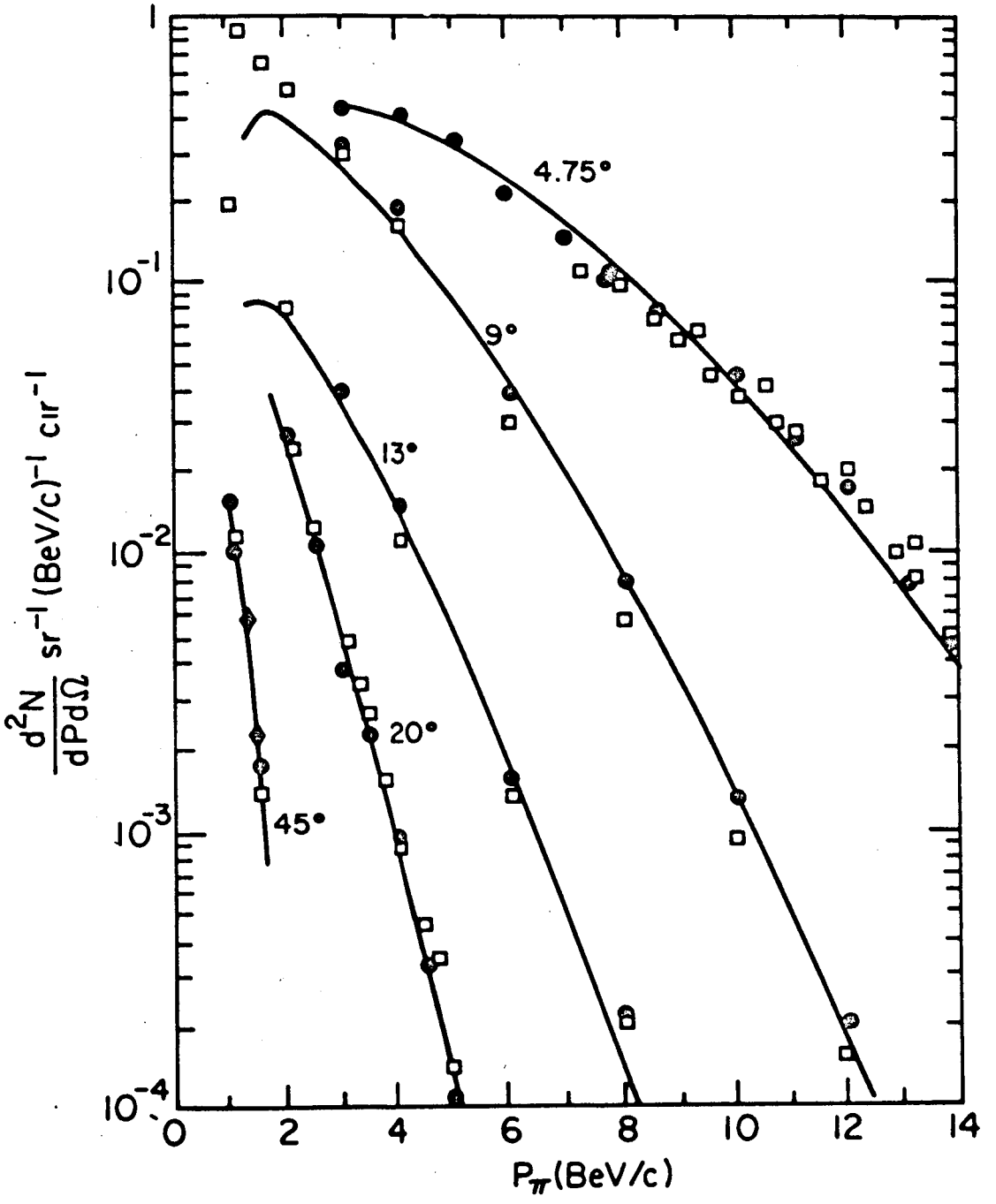
4.75°
9°
13°
20°
45°
$\frac{d^2N}{dPd\Omega}$ sr^{-1} (BeV/c)$^{-1}$ cir^{-1}
P_π(BeV/c)
1
10^{-1}
10^{-2}
10^{-3}
10^{-4}
0
2
4
6
8
10
12
14

Fig. 8

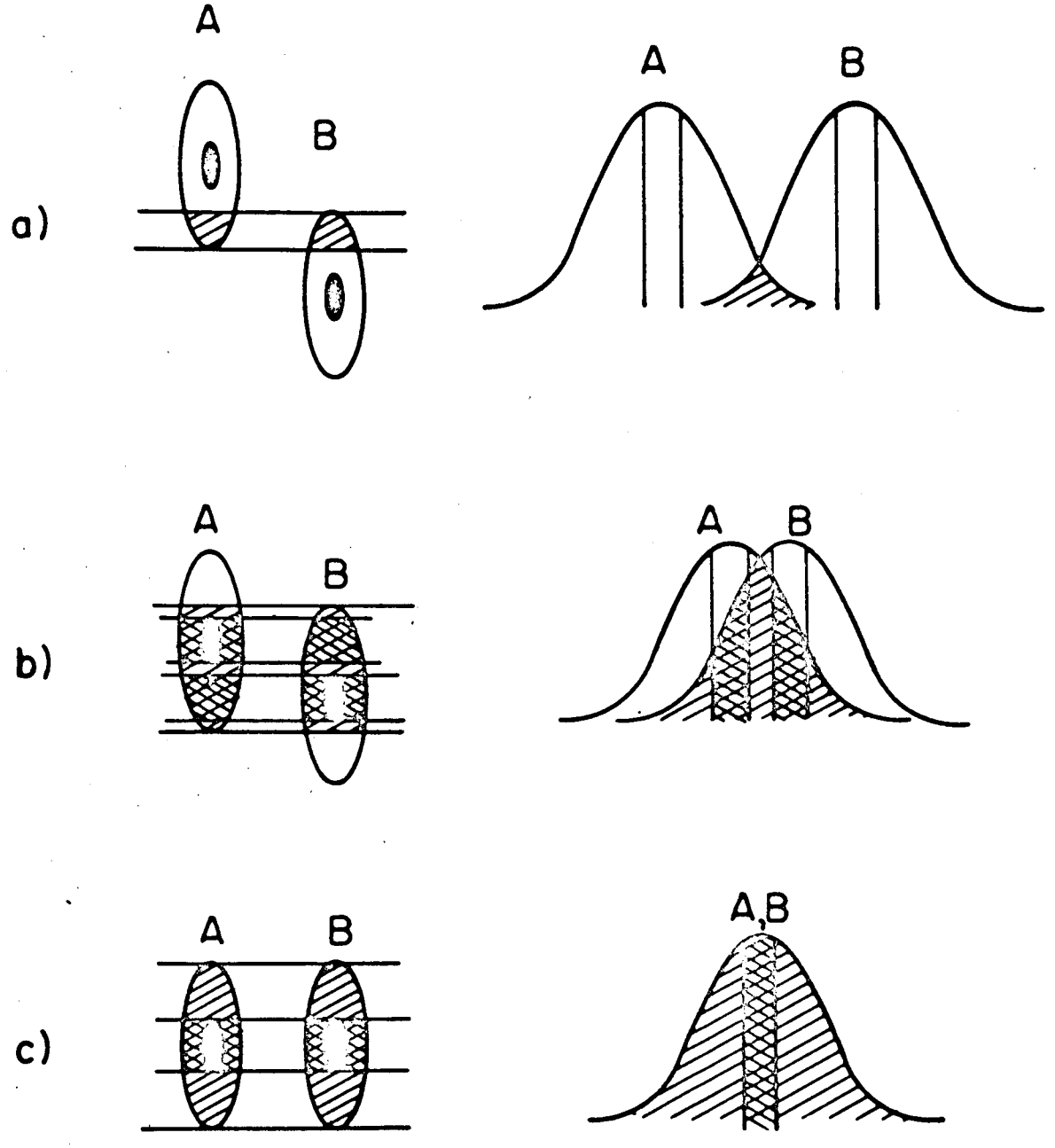

Fig. 9

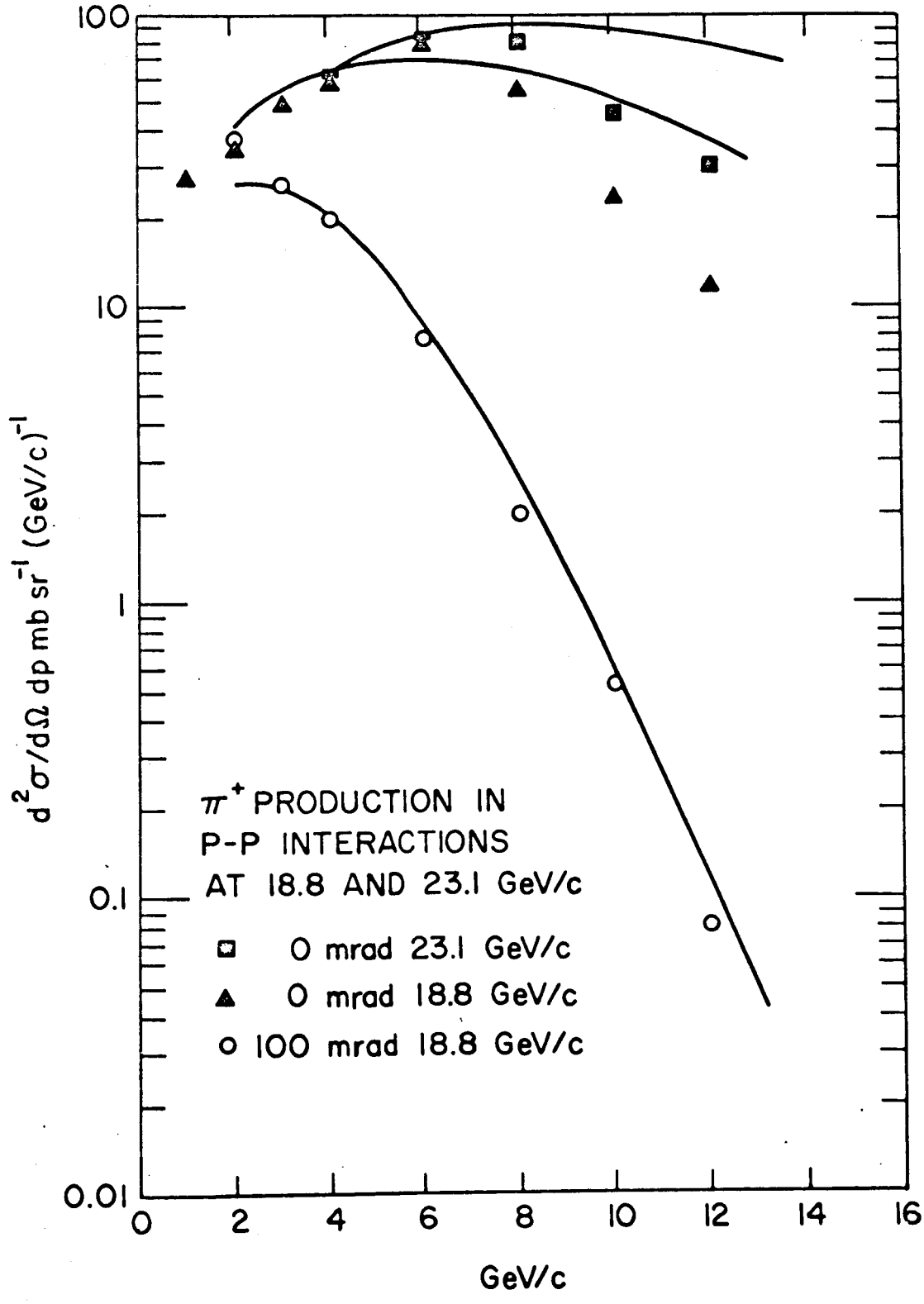
100
10
1
0.1
0.01
0
2
4
6
8
10
12
14
16
GeV/c
$d^2\sigma/d\Omega\, dp$ mb sr^{-1} $(GeV/c)^{-1}$
π^+ PRODUCTION IN
P-P INTERACTIONS
AT 18.8 AND 23.1 GeV/c
0 mrad 23.1 GeV/c
0 mrad 18.8 GeV/c
100 mrad 18.8 GeV/c

Fig. 10

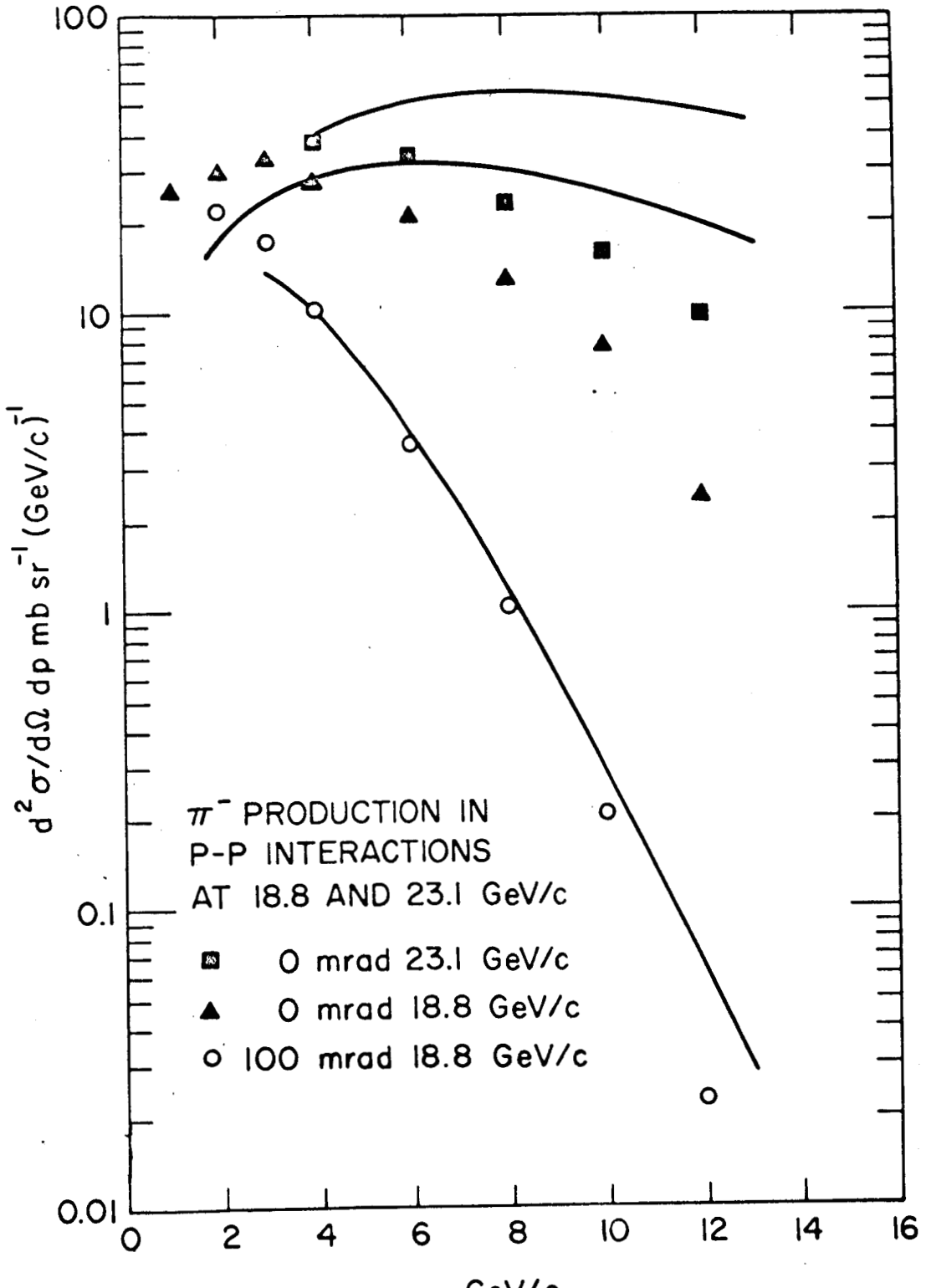
100
10
1
0.1
0.01
0
2
4
6
8
10
12
14
16
$d^2\sigma/d\Omega\, dp$ mb sr^{-1} $(GeV/c)^{-1}$
GeV/c
π^- PRODUCTION IN
P-P INTERACTIONS
AT 18.8 AND 23.1 GeV/c
0 mrad 23.1 GeV/c
0 mrad 18.8 GeV/c
100 mrad 18.8 GeV/c

Fig. 11

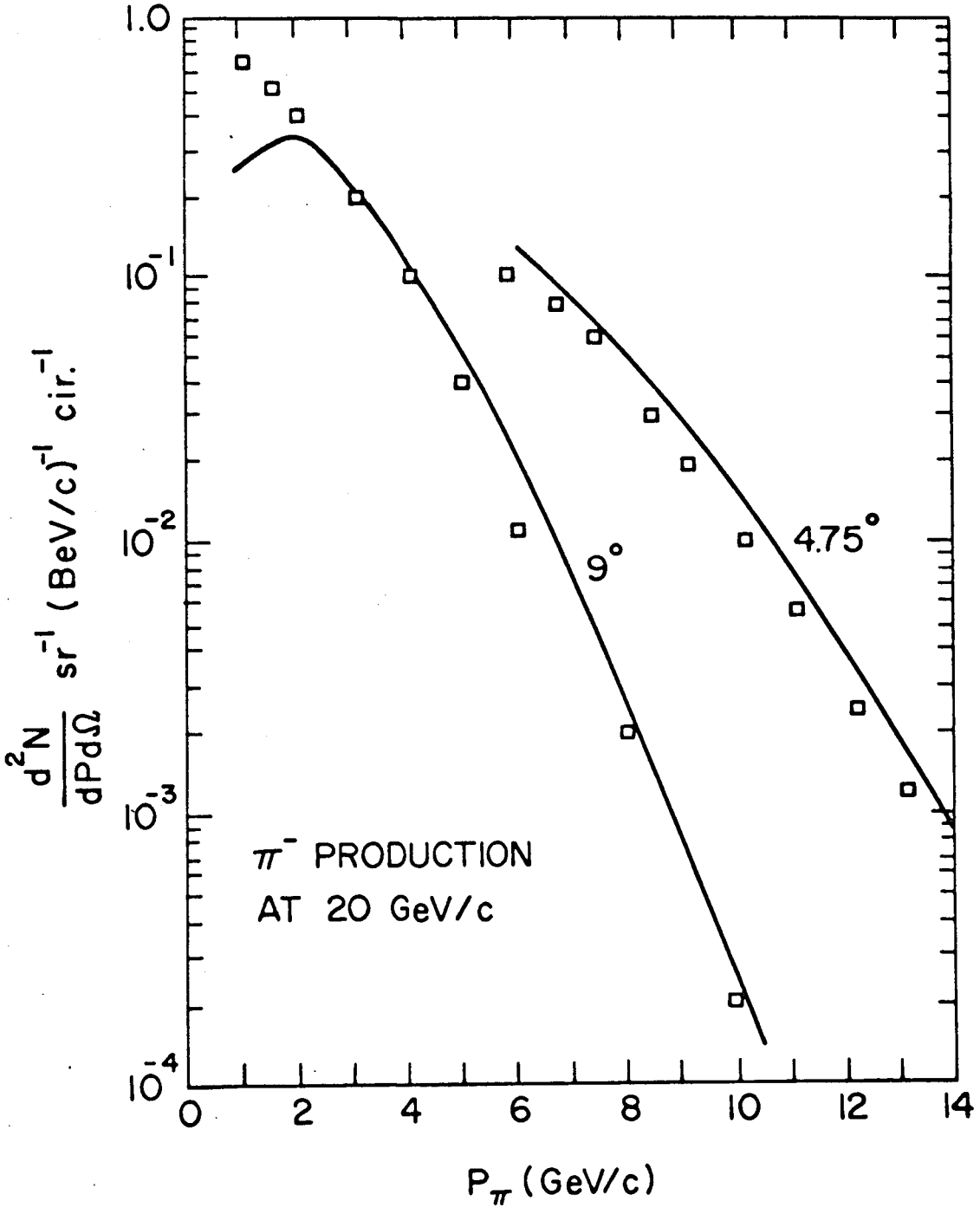
1.0
10^{-1}
10^{-2}
10^{-3}
10^{-4}
$\frac{d^2N}{dPd\Omega}$ sr^{-1} (BeV/c)$^{-1}$ cir.$^{-1}$
0
2
4
6
8
10
12
14
P_π (GeV/c)
π^- PRODUCTION
AT 20 GeV/c
9°
4.75°

Fig. 12

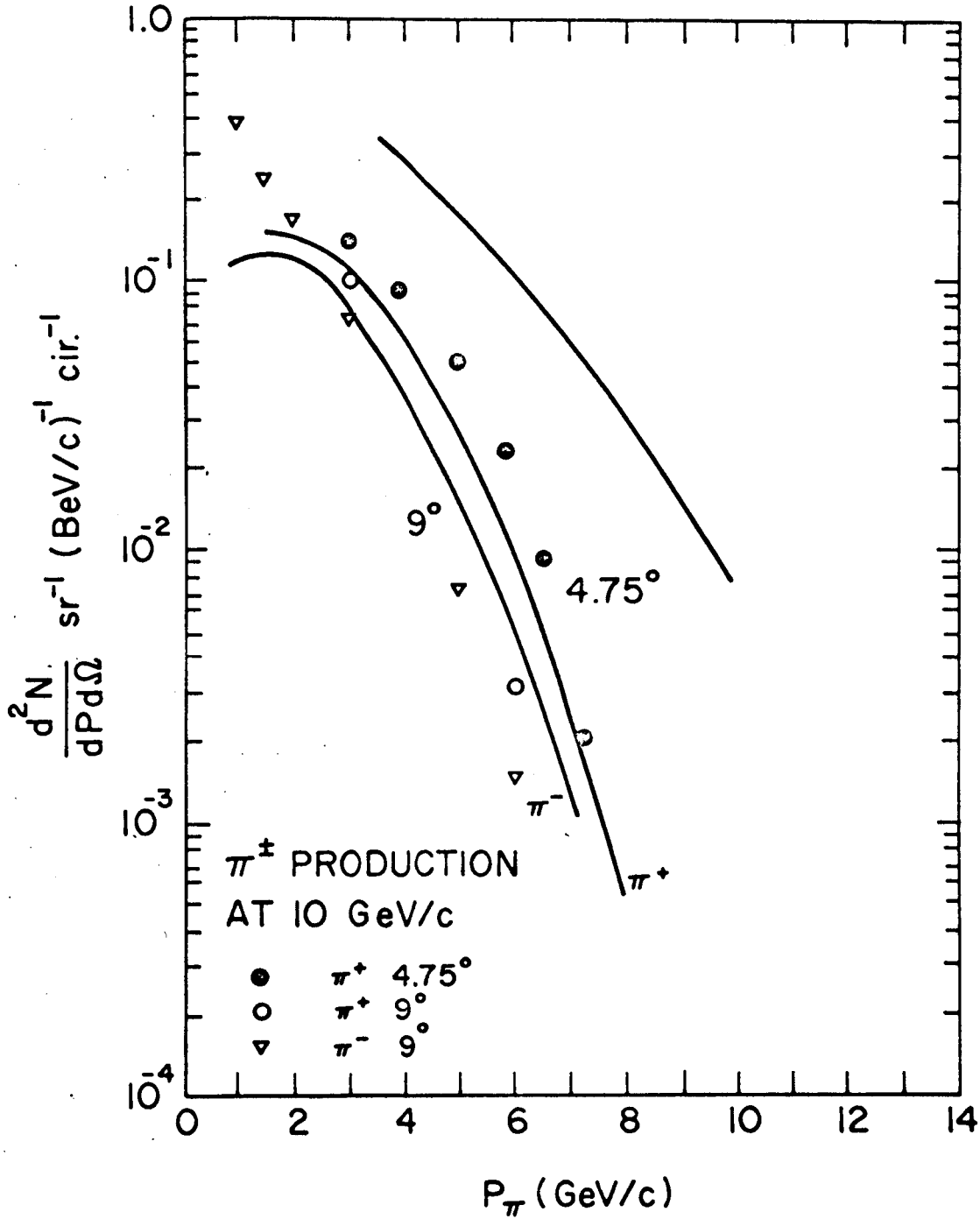
1.0
10^{-1}
10^{-2}
10^{-3}
10^{-4}
$\frac{d^2N}{dPd\Omega}$ sr^{-1} (BeV/c)$^{-1}$ cir.$^{-1}$
9°
4.75°
π^-
π^+
$\pi^\pm$ PRODUCTION
AT 10 GeV/c
π^+ 4.75°
π^+ 9°
π^- 9°
0
2
4
6
8
10
12
14
P_π (GeV/c)

Fig. 13

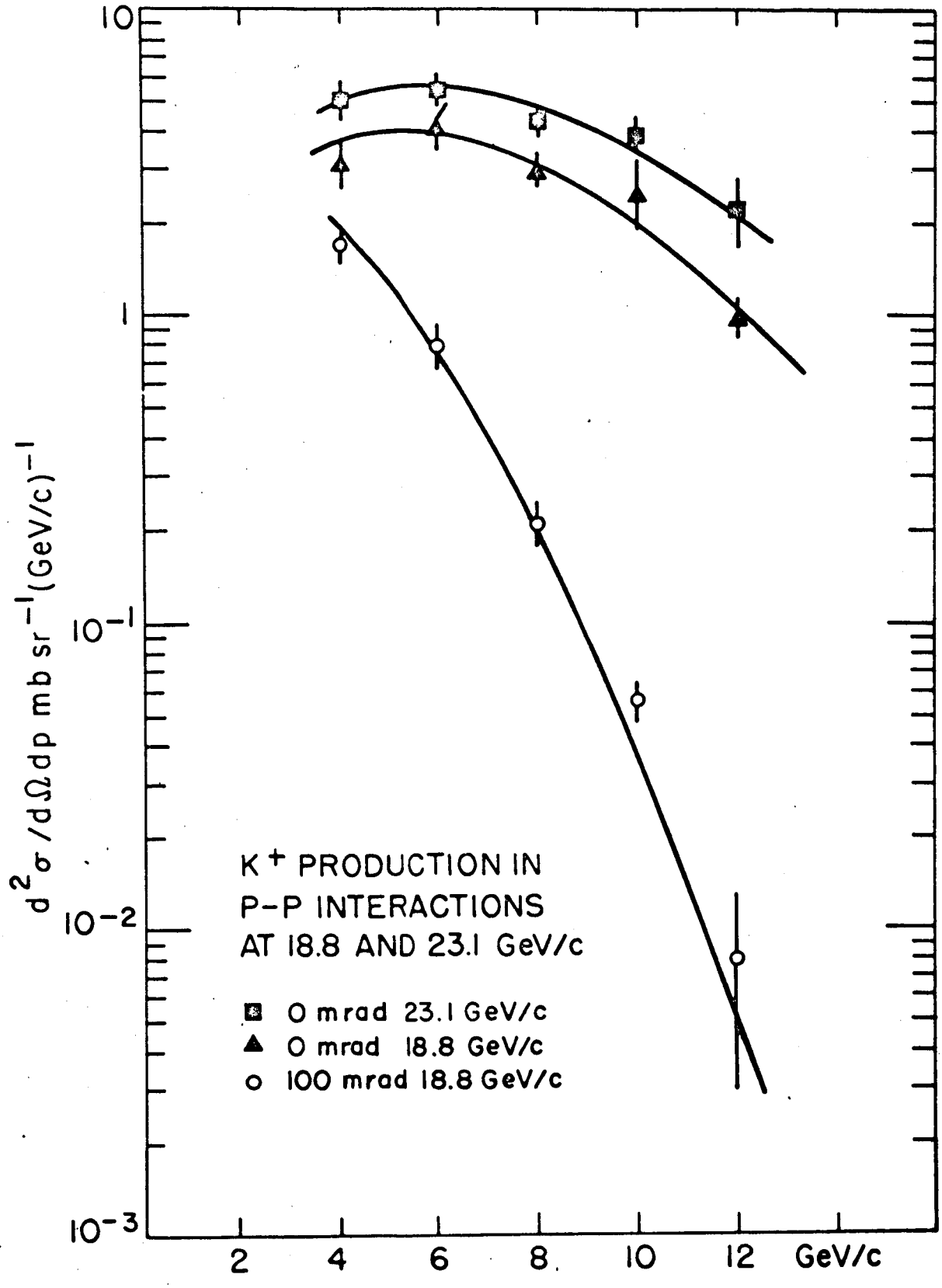
10
1
10^{-1}
10^{-2}
10^{-3}
$d^2\sigma/d\Omega dp$ mb $sr^{-1}(GeV/c)^{-1}$
2
4
6
8
10
12
GeV/c
K^+ PRODUCTION IN
P-P INTERACTIONS
AT 18.8 AND 23.1 GeV/c
0 mrad 23.1 GeV/c
0 mrad 18.8 GeV/c
100 mrad 18.8 GeV/c

Fig. 14

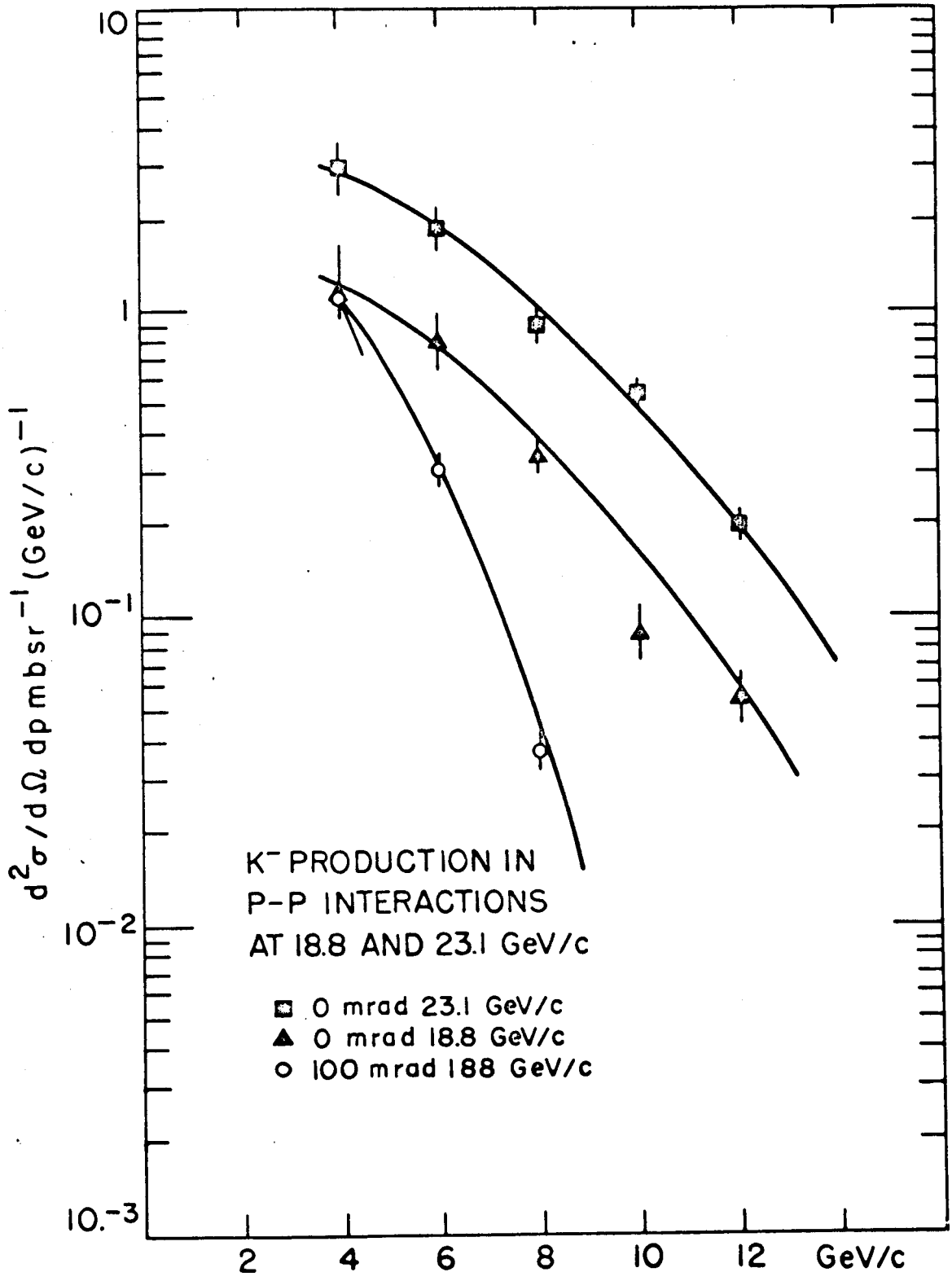
10
1
10^{-1}
10^{-2}
10^{-3}
$d^2\sigma/d\Omega\, dp\, mb\, sr^{-1}\, (GeV/c)^{-1}$
K⁻ PRODUCTION IN
P-P INTERACTIONS
AT 18.8 AND 23.1 GeV/c
0 mrad 23.1 GeV/c
0 mrad 18.8 GeV/c
100 mrad 188 GeV/c
2
4
6
8
10
12
GeV/c

Fig. 15

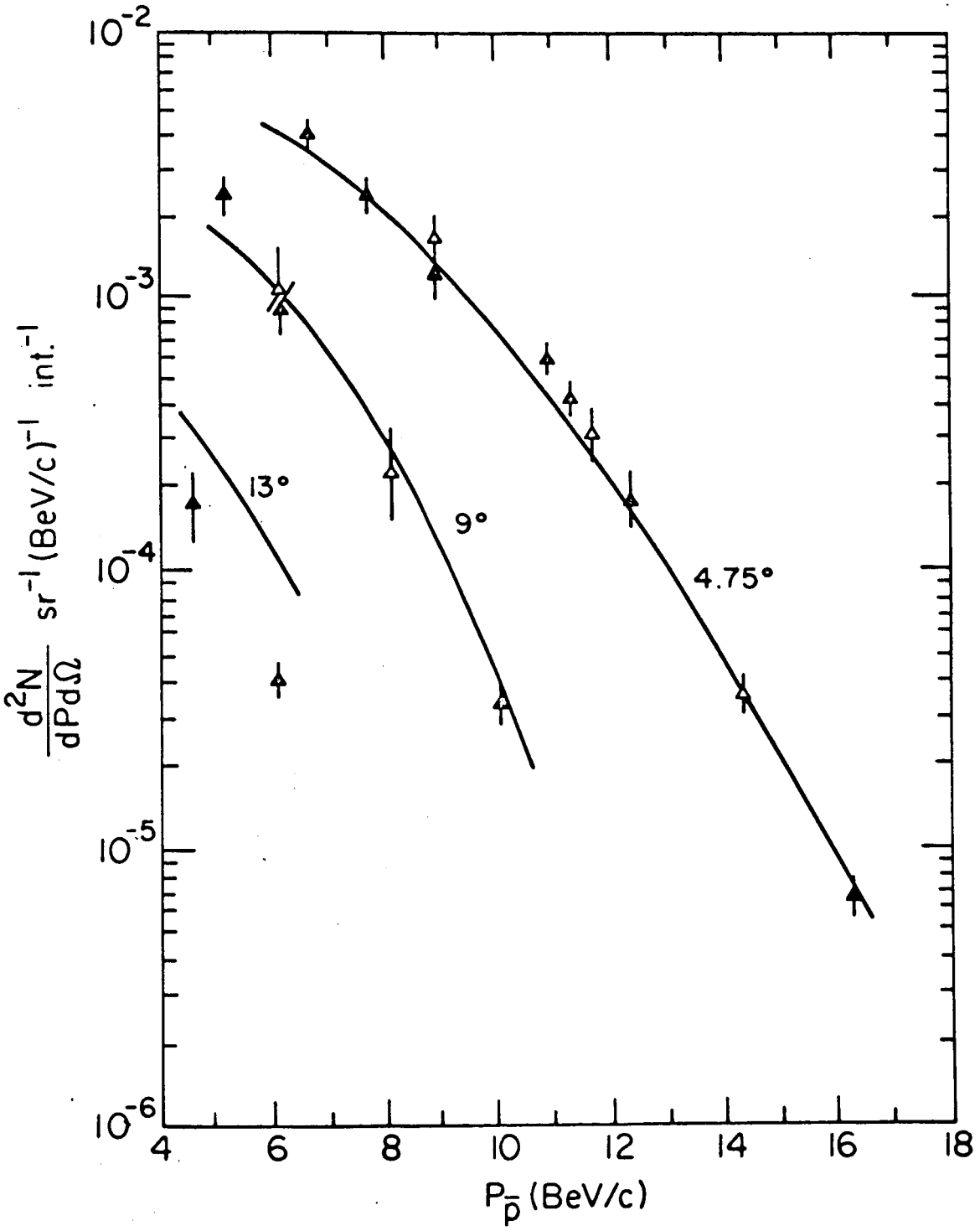
10^{-2}
10^{-3}
10^{-4}
10^{-5}
10^{-6}
$\frac{d^2N}{dPd\Omega}$ sr^{-1}(BeV/c)$^{-1}$ int.$^{-1}$
13°
9°
4.75°
4
6
8
10
12
14
16
18
$P_{\bar{p}}$ (BeV/c)

Fig. 16

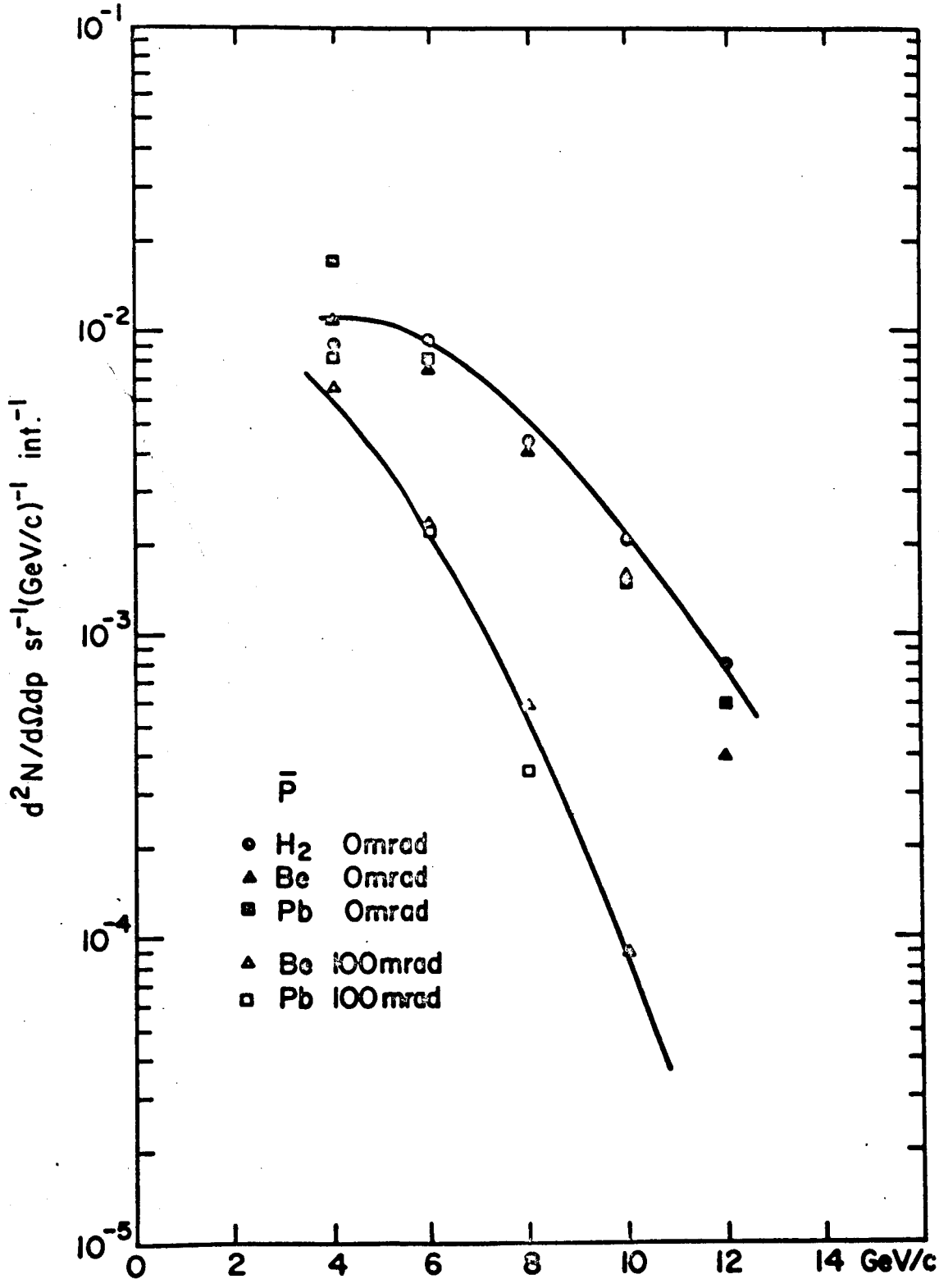
10^{-1}
10^{-2}
10^{-3}
10^{-4}
10^{-5}
$d^2N/d\Omega dp$ sr^{-1}(GeV/c)$^{-1}$ int.$^{-1}$
$\bar{P}$
H_2 Omrad
Be Omrad
Pb Omrad
Be 100mrad
Pb 100mrad
0
2
4
6
8
10
12
14 GeV/c

Fig. 17

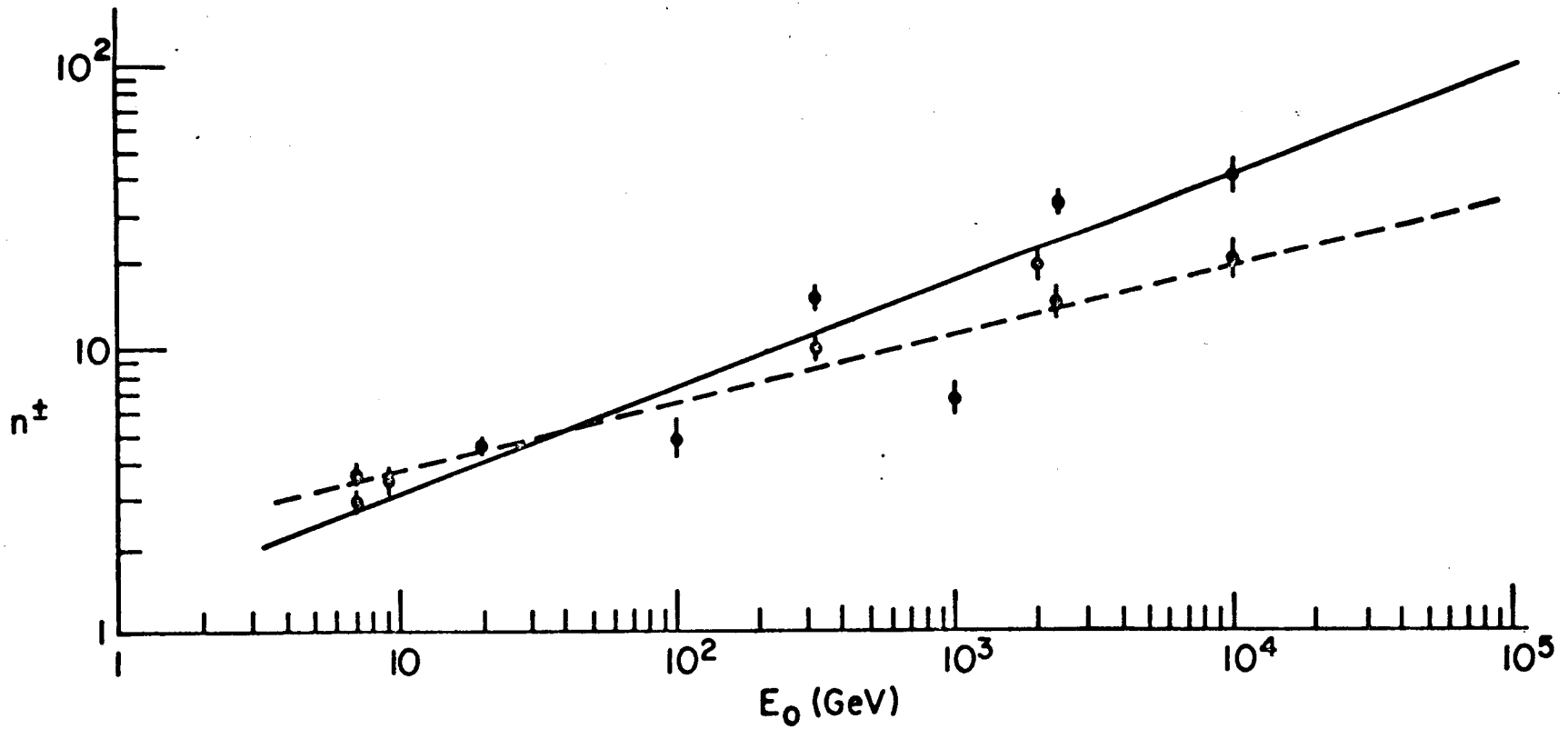

Fig. 18

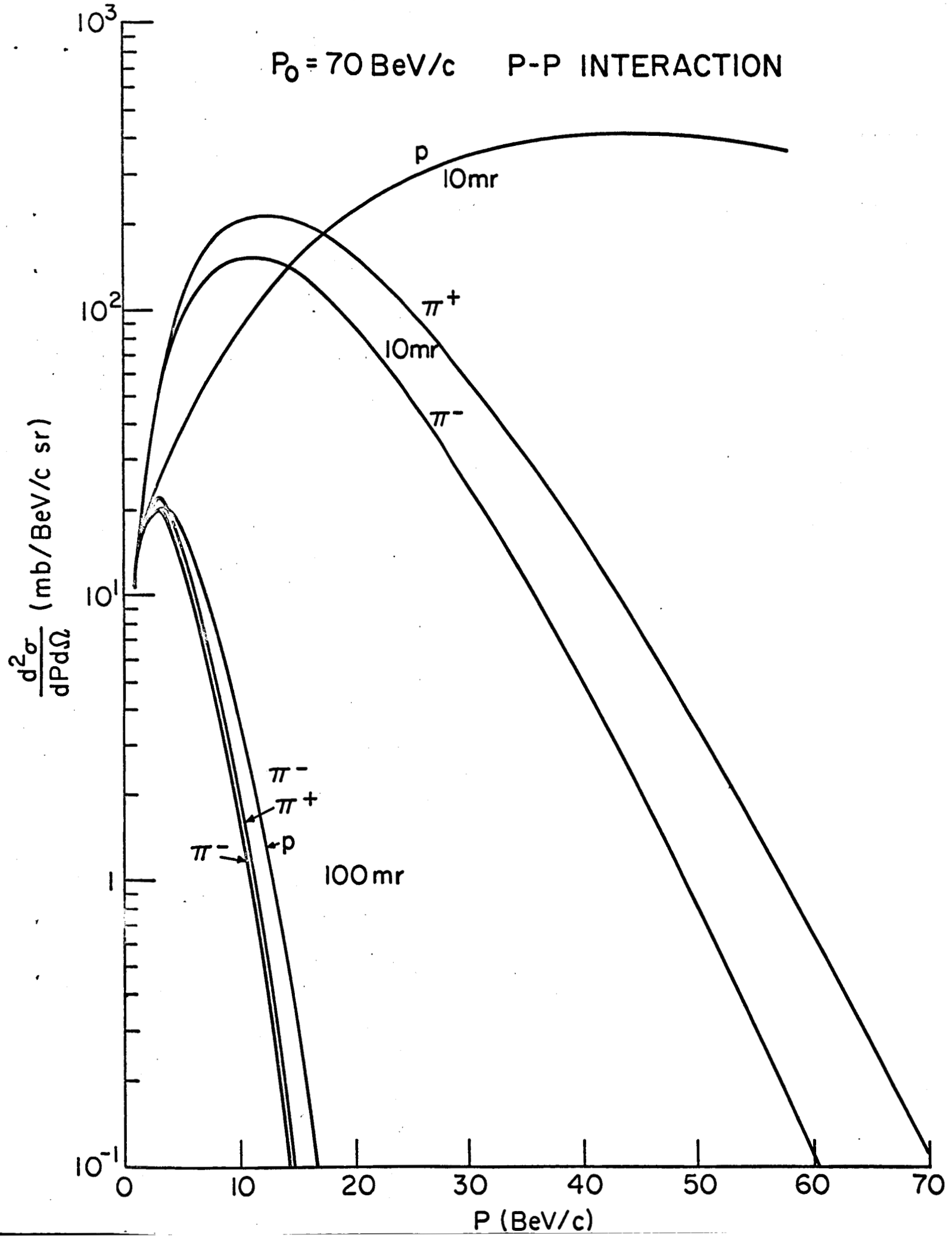
P_0 = 70 BeV/c P-P INTERACTION
p
10mr
π^+
10mr
π^-
π^-
π^+
p
π^-
100 mr
10^3
10^2
10^1
1
10^{-1}
$\frac{d^2\sigma}{dPd\Omega}$ (mb/BeV/c sr)
0
10
20
30
40
50
60
70
P (BeV/c)